The Width of the Martian Bow Shock and Implications on Thermalization

Sara Nesbit-Östman[1], Herbert Gunell[1], Maria Hamrin[1], Hermann Opgenoorth[2], and Laila Andersson[3]

[1]Umeå University
[2]Department of Physics, Umeå University
[3]Laboratory for Atmospheric and Space Physics (LASP)

May 2, 2023

Abstract

In theory the width of the quasi-perpendicular bow shock ramp is on the scale of a few electron inertial lengths, but as this work will show the quasi-perpendicular bow shock at Mars is often wider. This is important because it implies that the conditions at Mars create a behaviour at the shock which cannot be described by current theory. Furthermore, the width could affect processes at the shock such as energy transfer of the ions and their subsequent thermalization. To investigate the cause of the width, two sets of quasi-perpendicular bow shock crossings measured by MAVEN are compared, one of unusual width (average 370 km or 5r$_{gi}$), and one of typical width (average 30 km or 0.7r$_{gi}$). These sets are labeled wide and thin shocks respectively. It is seen that the wide shocks have no distinct overshoot and have a higher level of magnetic field fluctuations than the thin shocks. Factors that are known to affect the standoff distance, such as the magnetosonic Mach number and mass loading of the solar wind by planetary species, were found not to affect the width of the bow shock. It is found that the temperature of the solar wind plasma increases more as it passes through a wide than a thin shock, indicating that ions are thermalized to a larger extent than at thin shocks. The larger-than-predicted by theory width of the Martian quasi-perpendicular bow shock indicate that there are conditions at Mars which we do not yet understand.

The Width of the Martian Bow Shock and Implications on Thermalization

Sara Nesbit-Östman[1], Herbert Gunell[1], Maria Hamrin[1], Hermann Opgenoorth[1], Laila Andersson[2]

[1]Department of Physics, Umeå University, Umeå, Sweden
[2]Laboratory for Atmospheric and Space Physics, University of Colorado, Boulder, USA

Key Points:

- The quasi-perpendicular bow shock at Mars is often wider than what is predicted by theory.
- From theory the quasi-perpendicular ramp width is a few electron inertial lengths; in this study a sample of average $5\mathrm{r}_{gi}$ is shown.
- The proton temperature increases more across a wide shock compared to a thin shock, implying that wide shocks better thermalize protons.

Corresponding author: Sara Nesbit-Östman, `sara.ostman@umu.se`

Abstract

In theory the width of the quasi-perpendicular bow shock ramp is on the scale of a few electron inertial lengths, but as this work will show the quasi-perpendicular bow shock at Mars is often wider. This is important because it implies that the conditions at Mars create a behaviour at the shock which cannot be described by current theory. Furthermore, the width could affect processes at the shock such as energy transfer of the ions and their subsequent thermalization. To investigate the cause of the width, two sets of quasi-perpendicular bow shock crossings measured by MAVEN are compared, one of unusual width (average 370 km or 5r_{gi}), and one of typical width (average 30 km or 0.7r_{gi}). These sets are labeled wide and thin shocks respectively. It is seen that the wide shocks have no distinct overshoot and have a higher level of magnetic field fluctuations than the thin shocks. Factors that are known to affect the standoff distance, such as the magnetosonic Mach number and mass loading of the solar wind by planetary species, were found not to affect the width of the bow shock. It is found that the temperature of the solar wind plasma increases more as it passes through a wide than a thin shock, indicating that ions are thermalized to a larger extent than at thin shocks. The larger-than-predicted by theory width of the Martian quasi-perpendicular bow shock indicate that there are conditions at Mars which we do not yet understand.

1 Introduction

The bow shock is the first interaction region between the supersonic solar wind and the magnetosphere. Solar system bow shocks are important both for their role as laboratories from which we can extrapolate information on astrophysical shocks, and for their role in the evolution of planetary magnetospheres. In our solar system bow shocks have been identified for planets such as Earth, Mars and Venus as well as for comets, however the nature of the bow shock is different for these. At objects such as Earth (Behannon, 1968) and Jupiter (Valek et al., 2017) the bow shock is created in the interaction between the solar wind and the global magnetic field of the planet. For other bodies with no global magnetosphere, the bow shock is created in the interaction between the solar wind and the ionosphere, the magnetosphere of such objects we call induced magnetospheres (Luhmann et al., 2004). The bow shock is the boundary between the solar wind and the magnetosheath, where the magnetosheath is a region of pile-upped magnetic field where particles has slowed to subsonic speeds (Parks, 2015). Since the shock is created in the interaction with the ionosphere, the stand-off distance (distance from planet to shock) is shorter than for shocks which are created in the interaction of a strong global dipole field (Earth, Jupiter etc). Therefore the shock at Mars is smaller than that at for example Earth, and has a larger curvature radius. This affects the interaction of the solar wind and the shock, as the shock cannot be considered planar to the same extent as at Earth (Farris & Russell, 1994).

A possible consequence of this larger curvature radius is the width of the quasi-perpendicular bow shock seen at Mars. The quasi-perpendicular bow shock is typically a much thinner boundary than its quasi-parallel counterpart. The shock is called quasi-perpendicular where the angle between the interplanetary magnetic field (IMF) and the normal of the shock, θ_{bn}, is $45° < \theta_{bn} < 90°$ (Balogh & Treumann, 2013) (for a comparison between the quasi-perpendicular bow shock and a quasi-parallel bow shock see Appendix A). The quasi-perpendicular shock typically consists of a foot, a ramp, and an overshoot (Bale et al., 2005). The foot of the shock is created when ions are reflected at the shock and then accelerated parallel to the shock by the convective electric field of the solar wind. They constitute a current, which creates an increase in the magnetic field per Ampère's law. They gyrate less than an ion gyroradius before returning to the shock, which sets the thickness of the foot (Balikhin et al., 1995; Burne et al., 2021). The ramp is a current layer which gives rise to the change in the magnetic field. It is the thinnest structure of the shock, being a few electron inertial lengths wide (Newbury et al., 1998; le Roux et al., 2000; Hobara et al., 2010; Burne et al., 2021). Lastly there is the overshoot which is created due to the electrons being affected by the $\mathbf{E}\times\mathbf{B}$-drift along the shock, with the ions being unaffected due to the negligible width of the layer compared to the ion gyroradius. This once again constitutes a current, which causes an increase in the magnetic field; this increase is the overshoot. The width of the overshoot is on the scale of a few proton convected gyroradii (Burne et al., 2021).

At Mars however, the quasi-perpendicular bow shock often defies these predictions. The quasi-perpendicular bow shock at Mars is often wide, with a less discernible foot and overshoot. This is important because it implies that the conditions at Mars creates a behaviour at the shock which cannot be described by the above theory. Furthermore, the width could affect processes at the shock such as energy transfer of the ions and their subsequent thermalization. In this study 12 wide quasi-perpendicular bow shocks crossings have been chosen to be studied in more detail, in order to ascertain a possible cause of the widening. Given that the curvature radius possibly affects the width, parameters which affect the stand-off distance have been studied, since a larger stand-off distance implies less curvature. The magnetosonic Mach number has also been found to have an impact on bow shock stand-off distance at Mars with Edberg et al. (2010) finding that an increase in M_{MS} cause a decrease in bow shock altitude, with the relation being linear. Furthermore they found that at higher Mach numbers the bow shock showed more flaring. The relationship between bow shock location and M_{MS} was found to be similar to that at Venus, where a linear relationship has previously been found.

Another possible cause can be seen at the bow shocks of comets. Neubauer et al. (1993) found that bow shocks at comets often are wider and more gradual than that seen at planets, which is believed to be due to mass loading. Wide quasi-perpendicular bow shocks have been observed at comet Halley by the Giotto spacecraft (Coates, 1995). Due to the low gravity of the comet, the coma extends far around the comet and affects the solar wind far upstream from the comet. Due to the similarities between Mars and comets, such as the ratio of the gyroradius compared to the scale of the system, and an extended exosphere due to weak gravitational forces, it would be possible that something similar could affect the Martian bow shock.

In this paper we study 12 wide quasi-perpendicular events in detail, and compare these with 13 thin quasi-perpendicular bow shock crossing events. We assess whether M_{MS}, a factor that affect the stand-off distance, also affect the width, and we examine whether the location on the bow shock, such as closer to the nose or the flank, affect the width. Since wide bow shocks have been seen at comets due to mass loading, the upstream ion density have been studied to see if mass loading is more present for wide bow shocks. Finally, we hypothesize that there will be more time for thermalization of ions at the wide ramps. Therefore the ion temperature has been investigated to see if the ions at wide shocks are thermalized to a larger extent than at thin shocks. Specifically, we investigate whether there is a larger difference between upstream and downstream ion temperature for the wide events than for thin events.

2 Methodology, Data and Implementation

To investigate the cause for the width, 12 wide quasi-perpendicular events and 13 thin quasi-perpendicular events have been studied. The start and end times for these events can be found in Tables. B1 and B2 in Appendix B. The amount of events was limited by time constraints of the analysis of each event, where a larger amount of events would have been impractical for in-depth analysis. There were several criteria in the event selection. The wide events had to have a width greater than 200 km, have a discernible start and end, no large upstream amplitude fluctuations such that reformation of the shock is not mistaken for width (Madanian et al., 2020), and that the angle between the IMF and the normal of the shock, θ_{bn}, had to be larger than 65°, such that they were quasi-perpendicular. Furthermore, the ramp would appear wide were the spacecraft to travel along the shock. Therefore only events where the spacecraft travelled along the normal of the bow shock were chosen (with a maximum deviation of 30°). The criteria for the thin events were the same, except their widths had to be less than 100 km. The times for the wide and thin events can be found in Table B1 and B2 respectively. Thus, the width is a criterion for the classification, and we examine the difference in other properties of the wide and thin bow shocks.

To investigate whether causes which increase stand-off distance also affect width, the Magnetosonic mach number, M_{MS} and position of each crossing was investigated and compared between the two sets of events. Furthermore, to investigate whether the abnormal width was caused by mass loading, the upstream density of protons, alpha particles and atomic and molecular oxygen ions were similarly investigated and compared. Furthermore, the increased width of the shock gives more space for the particles be accelerated or decelerated by the potential drop at the shock, which raises the question of whether the shock width affects the thermalization at the shock. To this end the ion temperature was investigated to study whether the ions at wide shocks are thermalized to a larger extent than at thin shocks. The difference between the upstream and downstream temperature for all events were calculated, and then compared between the two sets.

The data of the study is from the MAVEN spacecraft during its first dayside season, 2014-11-16 to 2015-01-04. Magnetic field data was collected by the Magnetometer (MAG) (Connerney et al., 2015) onboard. MAG measures the vectorial magnetic field at a sampling frequency of 32 samples/s, and has a resolution of 0.05 nT. Ion data was measured by the Solar Wind Ion Analyzer (SWIA) (Halekas et al., 2015), a 2π non-mass electrostatic analyzer which provides onboard calculated moments. Care has been taken to not use data during the telemetry shift of the instrument which occurs at the bow shock. The onboard calculated second moment, i.e. the temperature, is calculated under the assumption that all ions are protons. The largest error is from alpha-particles, which due to their higher mass registers as higher energy particles, thereby raising the average temperature. To investigate how large this error is we have calculated our own temperature moment from the differential energy flux measured by SWIA, and manually removed the alpha particle energy range where they have been reasonably distinguished from the protons. The resulting temperature has not varied significantly from the onboard calculated temperature, and we have therefore drawn the conclusion that the SWIA onboard calculated temperature moment can be trusted, and have used it in our study. The differential particle flux of the electron energy spectra was measured by Solar Wind Electron Analyzer (SWEA) (Mitchell et al., 2016).

The upstream ion density for specific ion populations was calculated using data from the Suprathermal and Thermal Ion Composition (STATIC) energy-mass electrostatic analyzer (McFadden et al., 2015). STATIC resolves 8 masses, 32 energies, 16 azimuthal and 4 polar angles. From the differential particle flux the ion density, velocity and temperature were calculated as the 0th, 1st and 2nd moment of the velocity distribution function respectively. All quantities are presented in the MSO coordinate system, where the positive x-axis points from Mars toward the sun, the y-axis is opposite the direction of Mars' orbital motion, and the z-axis completes the right-handed system.

As mentioned in the introduction, the angle between the IMF and the normal of the bow shock, θ_{bn}, determines the dynamics of the shock. To ensure that the bow shocks are quasi-perpendicular it has been important to accurately determine θ_{bn}. To that end, two methods have been used, the local Mixed Mode Coplanarity method (Paschmann & Schwartz, 2000), and a global bow shock model by Ramstad et al. (2017), a solar wind and EUV dependent model. According to Lepidi et al. (1997), the Mixed Mode Coplanarity method together with minimum variance analysis were the most reliable single spacecraft methods for calculating the bow shock orientation, and aligned well with the-oretical predictions. As mentioned, in order to include only quasi-perpendicular bow shocks in this study, only events where both methods gave $\theta_{bn} > 65°$ have been used.

The width of the shock was calculated by multiplying the transit time of the spacecraft passing the shock with the speed of the spacecraft along the normal. The width is therefore defined as the width in normal direction of the shock. Three methods were trialled to estimate the transit time. One method was by manual inspection, where the transit time was estimated by choosing a beginning and end of the ramp, and where care was taken to not include the foot or overshoot. The transit time was calculated under the assumption of a stationary shock. An example of ramp transit time by manual inspection can be seen in panel a) in Fig. 1, where the shaded region marks the extent of the ramp. The two other methods were curve fitting methods, where two different equations were used to fit a curve onto the data. The first function was a hyperbolic tangent function:

$$f_0(t) = s_1 + \frac{1}{2}\Big(s_2 - s_1\Big)\left(1 + \tanh\left(\frac{t - t_m}{\Delta t}\right)\right) \tag{1}$$

where $s_{1,2}$ are 30 second averages of the up- and downstream magnetic field magnitude, t is time, t_m is the time for the mid point of the ramp, and Δt is the transit time for the spacecraft to pass the ramp. The other function tested follows f_0 of Eq. (1) with the addition of two Gaussian functions for modeling the foot and the overshoot of the bow shock:

$$f_1(t) = f_0(t) + a_1 \exp\left(\frac{-(t - b_1)^2}{2c_1^2}\right) + a_2 \exp\left(\frac{-(t - b_2)^2}{2c_2^2}\right) \tag{2}$$

where $a_{1,2}$, $b_{1,2}$ and $c_{1,2}$ are the height, center and width respectively of the Gaussian functions. Examples of the two curve fittings can be seen in Fig. 1, where panel b) shows the curve fitting of Eq. (1), and panel c) shows the curve fitting of Eq. (2). The blue shaded regions in the figure indicate the ramp width as determined by the curve fittings. It is interesting to see that the overshoot is much smaller in amplitude and much wider than what is associated with a typical overshoot, which makes one question whether this can be called an overshoot, or if it is a different phenomenon. In the end, calculating the width by manual inspection was chosen. The curve fittings were reliable for the most part, and will be interesting to use in a future study, but at times poorly modeled the bow shock. In a set of 12 events one or two poorly modeled bow shocks would have a large effect on the results, and therefore the manual inspection method was chosen.

3 Observations

3.1 Description of example events

An example of a wide quasi-perpendicular bow shock crossing can be seen in Fig. 2. For this event θ_{bn} was 65° with the mixed-mode coplanarity method, and 74° with the model by Ramstad et al. (2017), and the width was 607 km or 19.6 r_{gi}. The transit time used for calculating this width is seen in Fig. 2 as the region marked as "Shock". The spacecraft moved from the downstream side of the shock into the upstream solar wind. At approximately time 03:07:00 in panel (a) in Fig. 2 we see a broadening of the ion energy spectrogram, with the ions starting to decelerate. Further upstream in panel (b), around 03:08:20 we see the electrons be accelerated, forming a distribution both wider in energy and with a higher bulk energy than the upstream plasma. This happens further upstream for the electrons than for the ions, since the lower electron mass makes the typical length scales shorter for the electrons. Thus, the electrons are fully thermalized further upstream than the ions. In panel (c) we see the steepening of the magnetic field, further indicating that the spacecraft is crossing the bow shock. The ion and electron spectra in panels (a) and (b), and the ion moments in panels (d-f), are measured by SWIA, which has a telemetry mode shift upon crossing into the magnetosheath. In Fig. 2 such a shift happens at 03:09:50, and for a minute around this shift the calculated

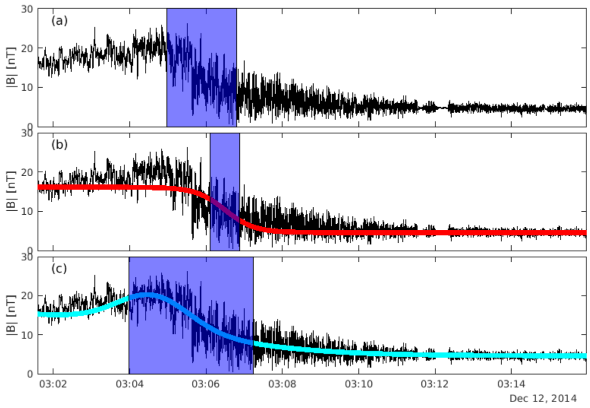

Figure 1: The three methods for determining the width of the ramp. The blue region in each panel is the ramp as determined by each method. In panel a) we see the interval that was chosen by manual inspection, in panel b) we see the curve fit of Eq. (1) and in panel c) we see the curve fit of Eq. (2).

moment will be in an ambiguous inbetween state, and should not be relied upon. We instead compare upstream and downstream ion moments to see whether the plasma has increased in density and temperature, and decreased in bulk velocity to confirm that the spacecraft has traveled into the magnetosheath. Outside ±30 s around the shift the ion moments can be trusted, it can be seen that the there is a gradual increase in density and a gradual decrease in velocity the same time we see a change in the energy spectrograms and the magnetic field. The relatively sharp increase in temperature in x-direction is likely due to the shift in telemetry mode, and for the temperature we instead look upstream and downstream for the change in temperature.

The average upstream magnetic field strength at this bow shock crossing is 4.7 nT, taken at a 30 s interval, and it is at this interval that averages for the ion density, velocity and temperature were also calculated. The regions where these values were taken can be seen in the colorbar in Fig. 2. For the temperature a downstream average was also calculated, in order to calculate the difference between the upstream and downstream temperature. The average upstream ion density was 1.85 cm^{-1}, the bulk velocity was 405 km/s, and the temperature in x-direction was 23 eV. The downstream average temperature in x-direction was 260 eV, making the ΔT of this event 237 eV. The 30 seconds of the intervals were a compromise between having a long enough averaging interval to lessen the effect of fluctuations, but not so long that too much time had passed since the bow shock crossing. The gradually increasing profiles are what characterize the wide bow shock ramp events: a broad steepening in the magnetic field and the plasma parameters. It is this behavior that is unexplained by current theory, as theory predicts that the width of a quasi-perpendicular bow shock ramp be of the size of a few electron inertial lengths (Newbury et al., 1998; le Roux et al., 2000; Hobara et al., 2010; Burne et al., 2021).

For comparison, an example of a thin quasi-perpendicular bow shock can be seen in Fig. 3. The width of this bow shock was 45 km or 6.2 r_{gi}, where the transit time used for calculating this width is seen in Fig. 3 as the region marked as "Shock". Here we see a sharp broadening of the energy spectrograms, and a sharp increase in magnetic field strength at around 04:11:40. The ion particle density and the ion bulk velocity similarly shows a quick increase and decrease respectively. For the temperature in x-direction we see an increase at the crossing and then a return to approximate solar wind temperatures. The amplitude of the magnetic field fluctuations during the shock transition are higher for the wide ramp in Fig. 2 than for the thin ramp in Fig. 3. In the case of the thin ramp (Fig. 3) there is an overshoot in both the magnetic field and density, whereas in for the wide ramp (Fig. 2) no such feature can be seen. Instead the large amplitude fluctuations in both density and magnetic field continue to be present also downstream of the shock itself. The energization of the protons and electrons are concentrated to the thin ramp, which gives less time for energization compared to the wide ramp. In the event in Fig. 3 the average upstream values of the magnetic field, ion density, velocity and temperature in x-direction was 9 nT, 5.2 cm^{-1}, 361 km/s, and 125 eV. The average downstream temperature in x-direction was 135 eV, making the ΔT of this event 10 eV.

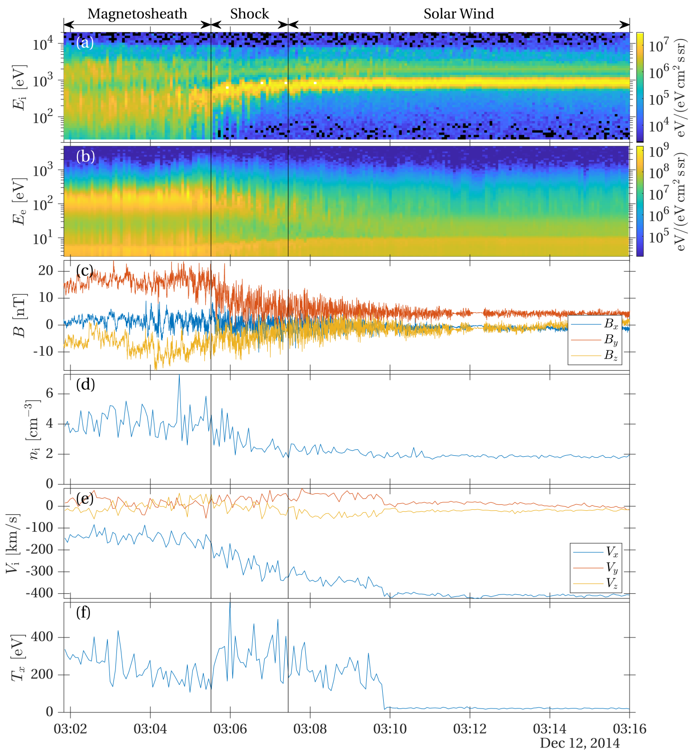

Figure 2: A wide quasi-perpendicular bow shock crossing with a width of 607 km or 19.6 r_{gi}. The spacecraft position at the time of the bow shock crossing (03:06:30) was (1.8, -0.2, 0.0)R$_M$. The panels show: a) the ion-energy spectrogram, b) the electron-energy spectrogram, (c) the magnetic field components, (d) the ion density, (e) the velocity components, and f) the temperature in x-direction.

3.2 Analysis of all events

To do some small scale statistics, 12 wide events and 13 thin events have been studied. In Fig. 4 we see where the bow shock crossings of the different events have taken place. We see an even distribution in position, with no discernible difference between wide and thin events. We do see that the majority of the bow shock crossings take place at the flank, this is likely due to orbit-bias, i.e. that MAVEN passed the bow shock at the flank during this time period. The lack of difference leads to the conclusion that the width of the ramp is not connected to location on the bow shock.

In Table 1 we see the average width and the standard deviation of the wide and thin ramps. The wide events are in the magnitude of the 100s of kilometers while the

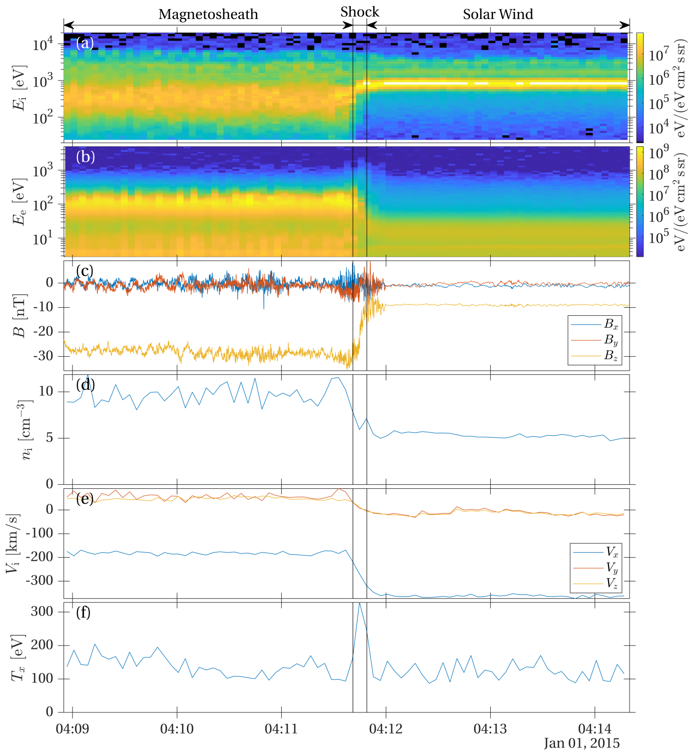

Figure 3: A thin quasi-perpendicular bow shock crossing with a width of 45 km or 6.2 r_{gi}. The spacecraft position at the time of the bow shock crossing (04:11:45) was (1.6, -1.1, 0.1)R$_M$. The panels show: a) the ion-energy spectrogram, b) the electron-energy spectrogram, (c) the magnetic field components, (d) the ion density, (e) the velocity components, and f) the temperature in x-direction.

thin events are in the 10s of kilometers. In terms of the proton gyroradius this is around 5 r_{gi} for the wide events, and 1 r_{gi} for the thin events. However the variance is very large as can be seen from the standard deviation where it is 6.7 r_{gi} for wide events and 1.6 r_{gi} for the thin events. There is however a significant difference.

It is known that the Magnetosonic Mach number, M$_{MS}$, affects stand-off distance (Edberg et al., 2010), and to see whether it also affects bow shock width we have compared M$_{MS}$ for wide and thin bow shocks. The average values of M$_{MS}$ together with one standard deviation can be found in Table 1. There were little difference to be found in M$_{MS}$ for wide and thin bow shock. Both kind of bow shocks display similar average and standard deviations in M$_{MS}$. Unlike the location of the shock, the thickness of the shock is seemingly independent of M$_{MS}$. The independence of M$_{MS}$ also aligns with the independence of location that was seen in Fig. 4, as a difference in M$_{MS}$ should correspond to a difference in bow shock stand-off distance as per previous research (Edberg et al., 2010).

In order to assess the importance of heavy ions for the nature of the shock we have computed the upstream particle densities of the ions H^+, H_2^+, O^+, and O_2^+. These can be found in Table 2. We find that the upstream particle density is higher for thin events for all ions. The average proton and atomic oxygen ion density is about twice as high, and the molecular oxygen ion density is about four times higher than for the wide events. The standard deviation is however on the scale of the average for all ions, which means there is a significant spread in density. The higher density for the thin events is not what

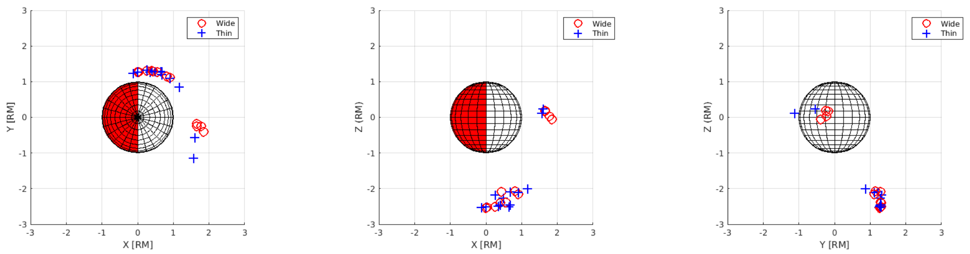

(a) YX-plane. (b) ZX-plane. (c) ZY-plane.

Figure 4: Position of bow shock crossing for the two type of events. The red circles are wide ramp events and the blue crosses are thin ramp events.

we would have expected in the case of mass loading being the cause of the wide ramps, as the higher density instead would have been expected for the wide ramps. This speaks against mass loading as being the cause of the width of the wide ramps.

Table 1: Thickness of the ramps of the wide and thin ramp events, as well as the magnetosonic Mach number. Values are given for the mean and the standard deviation (std).

	Wide		Thin	
	mean	std	mean	std
Thickness [km]	368	134	29	20
Thickness [r_{gi}]	5.4	6.7	0.7	1.6
M_{MS}	6.5	1.5	6.3	2.1

Table 2: Density of different ion species for wide and thin ramp events. Values are given for the mean and the standard deviation (std).

	Wide		Thin	
	mean	std	mean	std
H^+ [cm^{-3}]	2.5	1.9	4.4	1.9
H_2^+ [cm^{-3}]	0.2	0.1	0.3	0.2
O^+ [cm^{-3}]	0.04	0.05	0.1	0.15
O_2^+ [cm^{-3}]	0.05	0.07	0.2	0.2

Fig. 5 shows the difference between the downstream temperature and the upstream temperature in x-direction and plotted versus upstream velocity in x-direction. ΔT_x is expected to increase for increasing V_X, as there will be more energy available to be thermalized, and this can be seen for both wide and thin events. What can also be seen is that the wide events seem to more efficiently convert the kinetic energy to heat as the downstream temperatures are on average higher for the wide events. There is one outlier with a $\Delta T_x = 240$ eV, but even with that removed the average is higher. This is especially interesting given that the thin events had higher average upstream ion particle density, as that would imply there is more kinetic energy available. The higher energy transport for the wide events could be interesting for ionization of particles and particle escape, as it could implicate that more particles could be ionized and/or reach escape velocity.

4 Discussion

A caveat for this study is that it has been conducted under the assumption of a non-moving shock. Due to the limitations of single-spacecraft measurements it is difficult to estimate the movement of the shock. Methods such as estimating the velocity from the foot (Burne et al., 2021) has not been used here due to the difficulty in distinguishing the foot in the wide ramp events. This makes this line of questioning an excellent one to continue with multi-point measurements, this study aims to open the discussion of the width of the shock.

In spite of this being a single spacecraft study, one can have confidence that the wide shocks are indeed wide. A bow shock that rapidly moves back and forth would result in multiple bow shock crossings, which indeed can be observed in cases not included in this study. For a thin shock to be misinterpreted as a wide shock as those studied here, it would have to move at a speed just slightly faster than, and synchronised with, the spacecraft speed over the course of several minutes, and that is not likely. For example if a thin bow shock is 30 km wide, and the duration of the crossing of a wide shock is 3 minutes, then the relative spacecraft–bow shock velocity would have to be 0.17 km/s, which is much smaller than the typical spacecraft speed of 1.5-3 km/s at the bow shock. Could the opposite hypothesis be true: that all shocks are wide, some masked as thin by passing the spacecraft very quickly? This would require the bow shock to move in the range of 100 km/s which is possible. However, such a motion would not explain the differences in other properties between the shock types, such as fluctuation amplitudes and the presence or absence of an overshoot.

The cause for the bow shock thickness to differ between the different cases remains an open question. It is well known that the quasi-parallel and quasi-perpendicular shocks differ with the quasi-parallel having an extensive foreshock region, which potentially could be interpreted as a wider shock. In this study only quasi-perpendicular shocks are included, and therefore the difference between the parallel and perpendicular shocks cannot explain the observations. At comets, mass loading is important in determining the standoff distance of the bow shock (e.g., Koenders et al., 2013). The bow shocks encountered in the fast flybys of comets in the 1980s and 90s also had large widths. While this could lead to the speculation that the presence of heavy ions increases the bow shock width, that hypothesis cannot be confirmed by our data from Mars. As Table 2 shows, the density of heavy planetary ions is lower for the wide than for the thin shocks.

There is a potential across the shock, which slows the solar wind ions down while accelerating the electrons. The electron energy can be used to estimate this potential drop (Xu et al., 2021). It is seen in Figs. 2 and 3 that the energy of electrons and ions vary in the same way as the other quantities. The energy changes over a short distance for the thin ramps and over an outstretched region in the case of the wide ramps. This implies that also the potential drop changes over an extended region for the wide ramps and that the potential drop is concentrated in a thin layer for the thin ramps. The amplitude of the waves present is higher for the wide than thin ramps, and we suggest that in the wide ramps the waves may be able to balance the wider potential drop.

5 Summary

In this study wide quasi-perpendicular bow shocks have been compared to thin quasi-perpendicular bow shocks. The characteristics of the wide bow shocks show no difference in dependence of the bowshock's location with respect to the planet (sub-solar or flank) nor with respect to the magnetosonic Mach number. The wide bow shock events show lower upstream density than their thin counterparts, for protons, alpha particles, and atomic and molecular oxygen. With this in mind it is particularly interesting that they show a higher difference in upstream and downstream temperature, implying a higher

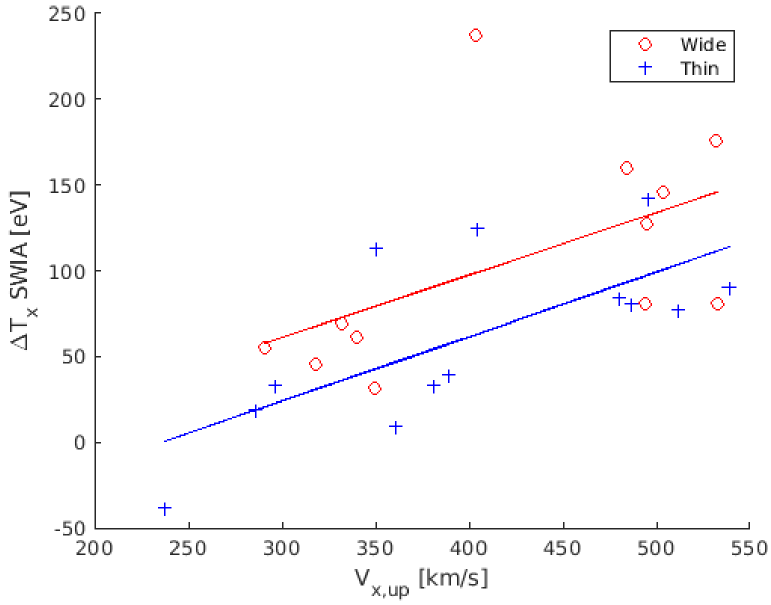

Figure 5: Difference in upstream and downstream temperature in x-direction for all events, $\Delta T_x = T_{down} - T_{up}$ over $V_{x,up}$.

rate of energy transfer at the wide bow shock. Future studies could look into larger amount of events, study the potential drop at the ramp, and perform wave analysis to see how waves affect the width of the shock. It will be of particular interest when multi-point measurements at Mars become available, as it will resolve some of the ambiguity of the shock movement and velocity. This study shows that current theory cannot fully describe the processes at the bow shock at Mars, and that these conditions affect not only bow shock width, but also increases the thermalization of ions at the Martian shock.

Appendix A Comparison between the quasi-parallel and quasi-perpendicular bow shock

To illustrate the difference between a wide quasi-perpendicular and a wide quasi-parallel bow shock we show a crossing of a wide quasi-parallel ramp in Fig. A1, which has $\theta_{bn} = 24°$ and $29°$ for the local and model method respectively. Due to the lack of discernible start and end of the ramp, it is hard to estimate the width, but an approximate value for this shock would be around 450 km. An important difference between wide quasi-parallel bow shock ramps and quasi-perpendicular ones is the amount of wave activity. At quasi-parallel bow shocks particles are reflected and escape upstream along the magnetic field lines, creating an extensive foreshock region. Due to the available free energy from the reflected particle beam there will be a multitude of instabilities and waves, and the solar wind will begin to be decelerated upstream of the bow shock. This makes the ramp appear very wide, often with no discernible start and end. At the quasi-perpendicular bow shock the reflected particles only reflect at most a gyroradius, and as such the solar wind in front of the shock less disturbed. At quasi-perpendicular bow shocks we can often discern a foot and an overshoot, coming from the reflected particles and sheet current respectively. These are not present at quasi-parallel shocks. In Fig. 2 we can see a wide quasi-perpendicular shock, with a wide ramp, but a discernible start and end, and a slight overshoot, though small. At the wide quasi-parallel shock in Fig. A1 there is large amplitude wave activity upstream and downstream, it is difficult to discern a beginning and end of the ramp, and no foot or overshoot can be identified.

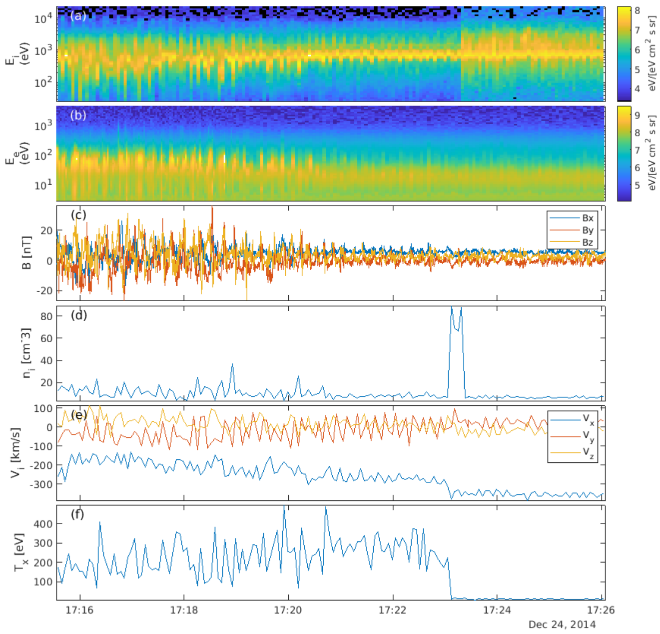

Figure A1: An approximately 450 km wide quasi-parallel bow shock crossing. The panels show: a) the ion-energy spectrogram, b) the electron-energy spectrogram, (c) the magnetic field components, (d) the ion density, (e) the velocity components, and f) the temperature in x-direction.

Appendix B Event start and end times

Table B1: Start and end times for wide events

Start event	End event
2014-12-03 09:58:56	2014-12-03 10:20:06
2014-12-04 22:45:55	2014-12-04 23:04:04
2014-12-07 05:29:28	2014-12-07 06:11:47
2014-12-08 21:00:49	2014-12-08 21:12:24
2014-12-10 09:42:36	2014-12-10 09:53:27
2014-12-12 03:01:35	2014-12-12 03:15:58
2014-12-15 11:04:47	2014-12-15 11:19:30
2014-12-16 17:06:30	2014-12-16 17:15:04
2014-12-18 07:46:08	2014-12-18 08:01:48
2014-12-29 00:42:09	2014-12-29 00:56:47
2015-01-02 14:29:10	2015-01-02 14:48:57
2015-01-04 07:40:40	2015-01-04 08:05:06

Table B2: Start and end times for thin events

Start event	End event
2014-11-16 13:09:23	2014-11-16 13:14:41
2014-12-03 01:02:37	2014-12-03 01:06:57
2014-12-05 03:29:22	2014-12-05 03:38:14
2014-12-05 16:46:07	2014-12-05 17:04:38
2014-12-12 14:09:29	2014-12-12 14:26:38
2014-12-13 03:48:06	2014-12-13 04:04:02
2014-12-17 15:52:56	2014-12-17 15:57:55
2014-12-22 22:00:06	2014-12-22 22:11:06
2014-12-23 07:16:52	2014-12-23 07:24:27
2015-01-01 04:08:52	2015-01-01 04:14:25
2015-01-01 15:43:13	2015-01-01 16:01:55
2015-01-04 03:13:54	2015-01-04 03:26:23
2015-01-13 16:07:22	2015-01-13 16:17:46

Acknowledgments

All MAVEN data are publicly available through the Planetary Data System (https://pds-ppi.igpp.ucla.edu/).

This work was funded by the Swedish National Space Board (SNSA, projects 108/18 and 194/19).

The authors would like to thank students J. Eriksson, E. Johansson, E. Rantala, P Sehlstedt, and F. Wikner at Umeå University for their development of the curve fitting method of Eq. (2).

References

Bale, S. D., Balikhin, M. A., Horbury, T. S., Krasnoselskikh, V. V., Kucharek, H., Möbius, E., … Thomsen, M. F. (2005, Jun 01). Quasi-perpendicular shock structure and processes. *Space Science Reviews*, *118*(1), 161–203. Retrieved from `https://doi.org/10.1007/s11214-005-3827-0` doi: 10.1007/s11214-005-3827-0

Balikhin, M., Krasnosselskikh, V., & Gedalin, M. (1995). The scales in quasiperpendicular shocks. *Advances in Space Research*, *15*(8), 247-260. Retrieved from `https://www.sciencedirect.com/science/article/pii/027311779400105A` (Proceedings of the D2.1 Symposium of COSPAR Scientific Commission D) doi: https://doi.org/10.1016/0273-1177(94)00105-A

Balogh, A., & Treumann, R. A. (2013). *Physics of collisionless shocks* (Vol. 12). Springer, New York, NY. doi: 10.1007/978-1-4614-6099-2

Behannon, K. W. (1968). Mapping of the earth's bow shock and magnetic tail by explorer 33. *Journal of Geophysical Research (1896-1977)*, *73*(3), 907-930. Retrieved from `https://agupubs.onlinelibrary.wiley.com/doi/abs/10.1029/JA073i003p00907` doi: https://doi.org/10.1029/JA073i003p00907

Burne, S., Bertucci, C., Mazelle, C., Morales, L. F., Meziane, K., Halekas, J., … Penou, E. (2021). The structure of the Martian quasi-perpendicular supercritical shock as seen by MAVEN. *Journal of Geophysical Research (Space Physics)*,

126(9), e2020JA028938. doi: 10.1029/2020JA028938
Coates, A. J. (1995, March). Heavy ion effects on cometary shocks. *Advances in Space Research*, *15*(8-9), 403–413. doi: 10.1016/0273-1177(94)00125-K
Connerney, J. E. P., Espley, J., Lawton, P., Murphy, S., Odom, J., Oliversen, R., & Sheppard, D. (2015). The maven magnetic field investigation. *Space Sci Rev*, *195*, 257–291. doi: https://doi.org/10.1007/s11214-015-0169-4
Edberg, N. J. T., Lester, M., Cowley, S. W. H., Brain, D. A., Fränz, M., & Barabash, S. (2010). Magnetosonic mach number effect of the position of the bow shock at mars in comparison to venus. *Journal of Geophysical Research: Space Physics*, *115*(A7). Retrieved from https://agupubs.onlinelibrary.wiley.com/doi/abs/10.1029/2009JA014998 doi: https://doi.org/10.1029/2009JA014998
Farris, M. H., & Russell, C. T. (1994). Determining the standoff distance of the bow shock: Mach number dependence and use of models. *Journal of Geophysical Research: Space Physics*, *99*(A9), 17681-17689. Retrieved from https://agupubs.onlinelibrary.wiley.com/doi/abs/10.1029/94JA01020 doi: https://doi.org/10.1029/94JA01020
Halekas, J. S., Taylor, E. R., Dalton, G., Johnson, G., Curtis, D. W., McFadden, J. P., … Jakosky, B. M. (2015). The solar wind ion analyzer for maven. *Space Sci Rev*, *195*, 125–151. doi: https://doi.org/10.1007/s11214-013-0029-z
Hobara, Y., Balikhin, M., Krasnoselskikh, V., Gedalin, M., & Yamagishi, H. (2010). Statistical study of the quasi-perpendicular shock ramp widths. *Journal of Geophysical Research: Space Physics*, *115*(A11). Retrieved from https://agupubs.onlinelibrary.wiley.com/doi/abs/10.1029/2010JA015659 doi: https://doi.org/10.1029/2010JA015659
Koenders, C., Glassmeier, K.-H., Richter, I., Motschmann, U., & Rubin, M. (2013, October). Revisiting cometary bow shock positions. *Planet. Space Sci.*, *87*, 85–95. doi: 10.1016/j.pss.2013.08.009
Lepidi, S., Villante, U., & Lazarus, A. J. (1997). Single spacecraft identification of the bow shock orientation and speed: A comparison between different methods. *Il nuovo cimento*, *20*(6), 911-922. Retrieved from http://eprints.bice.rm.cnr.it/id/eprint/12401
le Roux, J. A., Fichtner, H., Zank, G. P., & Ptuskin, V. S. (2000). Self-consistent acceleration of multiply reflected pickup ions at a quasi-perpendicular solar wind termination shock: a fluid approach. *Journal of Geophysical Research: Space Physics*, *105*(A6), 12557-12577. Retrieved from https://agupubs.onlinelibrary.wiley.com/doi/abs/10.1029/1999JA000273 doi: https://doi.org/10.1029/1999JA000273
Luhmann, J., Ledvina, S., & Russell, C. (2004). Induced magnetospheres. *Advances in Space Research*, *33*(11), 1905-1912. Retrieved from https://www.sciencedirect.com/science/article/pii/S0273117704000158 (Comparative Magnetospheres) doi: https://doi.org/10.1016/j.asr.2003.03.031
Madanian, H., Schwartz, S. J., Halekas, J. S., & Wilson III, L. B. (2020). Nonstationary quasiperpendicular shock and ion reflection at Mars. *Geophys. Res. Lett.*, *47*(11), e2020GL088309. doi: 10.1029/2020GL088309
McFadden, J. P., Kortmann, O., Curtis, D., Dalton, G., Johnson, G., Abiad, R., … M., J. (2015). Maven suprathermal and thermal ion compostion (static) instrument. *Space Sci Review*, *195*, 199–256. doi: https://doi.org/10.1007/s11214-015-0175-6
Mitchell, D. L., Mazelle, C., Sauvaud, J.-A., Thocaven, J.-J., Rouzaud, J., Fedorov, A., … Jakosky, B. M. (2016). The maven solar wind electron analyzer. *Space Sci Review*, *200*, 495–528. doi: https://doi.org/10.1007/s11214-015-0232-1
Neubauer, F. M., Marschall, H., Pohl, M., Glassmeier, K.-H., Musmann, G., Mariani, F., … Ungstrup, E. (1993, February). First results from the Giotto magnetometer experiment during the P/Grigg-Skjellerup encounter. *Astron-*

omy & Astrophysics, *268*, L5–L8.
Newbury, J. A., Russell, C. T., & Gedalin, M. (1998). The ramp widths of high-mach-number, quasi-perpendicular collisionless shocks. *Journal of Geophysical Research: Space Physics*, *103*(A12), 29581-29593. Retrieved from `https://agupubs.onlinelibrary.wiley.com/doi/abs/10.1029/1998JA900024` doi: https://doi.org/10.1029/1998JA900024
Parks, G. (2015). Magnetosphere. In G. R. North, J. Pyle, & F. Zhang (Eds.), *Encyclopedia of atmospheric sciences (second edition)* (Second Edition ed., p. 309-315). Oxford: Academic Press. Retrieved from `https://www.sciencedirect.com/science/article/pii/B9780123822253002115` doi: https://doi.org/10.1016/B978-0-12-382225-3.00211-5
Paschmann, G., & Schwartz, S. J. (2000, February). ISSI Book on Analysis Methods for Multi-Spacecraft Data. In R. A. Harris (Ed.), *Cluster-ii workshop multiscale / multipoint plasma measurements* (Vol. 449, p. 99).
Ramstad, R., Barabash, S., Futaana, Y., & Holmström, M. (2017). Solar wind- and euv-dependent models for the shapes of the martian plasma boundaries based on mars express measurements. *Journal of Geophysical Research: Space Physics*, *122*(7), 7279-7290. Retrieved from `https://agupubs.onlinelibrary.wiley.com/doi/abs/10.1002/2017JA024098` doi: https://doi.org/10.1002/2017JA024098
Valek, P. W., Thomsen, M. F., Allegrini, F., Bagenal, F., Bolton, S., Connerney, J., ... Wilson, R. J. (2017). Hot flow anomaly observed at jupiter's bow shock. *Geophysical Research Letters*, *44*(16), 8107-8112. Retrieved from `https://agupubs.onlinelibrary.wiley.com/doi/abs/10.1002/2017GL073175` doi: https://doi.org/10.1002/2017GL073175
Xu, S., Schwartz, S. J., Mitchell, D. L., Horaites, K., Andersson, L., Halekas, J., ... Gruesbeck, J. R. (2021). Cross-shock electrostatic potentials at Mars inferred from MAVEN measurements. *Journal of Geophysical Research: Space Physics*, *126*(3), e2020JA029064. doi: 10.1029/2020JA029064

The Width of the Martian Bow Shock and Implications on Thermalization

Sara Nesbit-Östman[1], Herbert Gunell[1], Maria Hamrin[1], Hermann Opgenoorth[1], Laila Andersson[2]

[1]Department of Physics, Umeå University, Umeå, Sweden
[2]Laboratory for Atmospheric and Space Physics, University of Colorado, Boulder, USA

Key Points:

- The quasi-perpendicular bow shock at Mars is often wider than what is predicted by theory.
- From theory the quasi-perpendicular ramp width is a few electron inertial lengths; in this study a sample of average $5r_{gi}$ is shown.
- The proton temperature increases more across a wide shock compared to a thin shock, implying that wide shocks better thermalize protons.

Corresponding author: Sara Nesbit-Östman, `sara.ostman@umu.se`

Abstract

In theory the width of the quasi-perpendicular bow shock ramp is on the scale of a few electron inertial lengths, but as this work will show the quasi-perpendicular bow shock at Mars is often wider. This is important because it implies that the conditions at Mars create a behaviour at the shock which cannot be described by current theory. Furthermore, the width could affect processes at the shock such as energy transfer of the ions and their subsequent thermalization. To investigate the cause of the width, two sets of quasi-perpendicular bow shock crossings measured by MAVEN are compared, one of unusual width (average 370 km or 5r_{gi}), and one of typical width (average 30 km or 0.7r_{gi}). These sets are labeled wide and thin shocks respectively. It is seen that the wide shocks have no distinct overshoot and have a higher level of magnetic field fluctuations than the thin shocks. Factors that are known to affect the standoff distance, such as the magnetosonic Mach number and mass loading of the solar wind by planetary species, were found not to affect the width of the bow shock. It is found that the temperature of the solar wind plasma increases more as it passes through a wide than a thin shock, indicating that ions are thermalized to a larger extent than at thin shocks. The larger-than-predicted by theory width of the Martian quasi-perpendicular bow shock indicate that there are conditions at Mars which we do not yet understand.

1 Introduction

The bow shock is the first interaction region between the supersonic solar wind and the magnetosphere. Solar system bow shocks are important both for their role as laboratories from which we can extrapolate information on astrophysical shocks, and for their role in the evolution of planetary magnetospheres. In our solar system bow shocks have been identified for planets such as Earth, Mars and Venus as well as for comets, however the nature of the bow shock is different for these. At objects such as Earth (Behannon, 1968) and Jupiter (Valek et al., 2017) the bow shock is created in the interaction between the solar wind and the global magnetic field of the planet. For other bodies with no global magnetosphere, the bow shock is created in the interaction between the solar wind and the ionosphere, the magnetosphere of such objects we call induced magnetospheres (Luhmann et al., 2004). The bow shock is the boundary between the solar wind and the magnetosheath, where the magnetosheath is a region of pile-upped magnetic field where particles has slowed to subsonic speeds (Parks, 2015). Since the shock is created in the interaction with the ionosphere, the stand-off distance (distance from planet to shock) is shorter than for shocks which are created in the interaction of a strong global dipole field (Earth, Jupiter etc). Therefore the shock at Mars is smaller than that at for example Earth, and has a larger curvature radius. This affects the interaction of the solar wind and the shock, as the shock cannot be considered planar to the same extent as at Earth (Farris & Russell, 1994).

A possible consequence of this larger curvature radius is the width of the quasi-perpendicular bow shock seen at Mars. The quasi-perpendicular bow shock is typically a much thinner boundary than its quasi-parallel counterpart. The shock is called quasi-perpendicular where the angle between the interplanetary magnetic field (IMF) and the normal of the shock, θ_{bn}, is $45° < \theta_{bn} < 90°$ (Balogh & Treumann, 2013) (for a comparison between the quasi-perpendicular bow shock and a quasi-parallel bow shock see Appendix A). The quasi-perpendicular shock typically consists of a foot, a ramp, and an overshoot (Bale et al., 2005). The foot of the shock is created when ions are reflected at the shock and then accelerated parallel to the shock by the convective electric field of the solar wind. They constitute a current, which creates an increase in the magnetic field per Ampère's law. They gyrate less than an ion gyroradius before returning to the shock, which sets the thickness of the foot (Balikhin et al., 1995; Burne et al., 2021). The ramp is a current layer which gives rise to the change in the magnetic field. It is the thinnest structure of the shock, being a few electron inertial lengths wide (Newbury et al., 1998; le Roux et al., 2000; Hobara et al., 2010; Burne et al., 2021). Lastly there is the overshoot which is created due to the electrons being affected by the $\mathbf{E}\times\mathbf{B}$-drift along the shock, with the ions being unaffected due to the negligible width of the layer compared to the ion gyroradius. This once again constitutes a current, which causes an increase in the magnetic field; this increase is the overshoot. The width of the overshoot is on the scale of a few proton convected gyroradii (Burne et al., 2021).

At Mars however, the quasi-perpendicular bow shock often defies these predictions. The quasi-perpendicular bow shock at Mars is often wide, with a less discernible foot and overshoot. This is important because it implies that the conditions at Mars creates a behaviour at the shock which cannot be described by the above theory. Furthermore, the width could affect processes at the shock such as energy transfer of the ions and their subsequent thermalization. In this study 12 wide quasi-perpendicular bow shocks crossings have been chosen to be studied in more detail, in order to ascertain a possible cause of the widening. Given that the curvature radius possibly affects the width, parameters which affect the stand-off distance have been studied, since a larger stand-off distance implies less curvature. The magnetosonic Mach number has also been found to have an impact on bow shock stand-off distance at Mars with Edberg et al. (2010) finding that an increase in M_{MS} cause a decrease in bow shock altitude, with the relation being linear. Furthermore they found that at higher Mach numbers the bow shock showed more flaring. The relationship between bow shock location and M_{MS} was found to be similar to that at Venus, where a linear relationship has previously been found.

Another possible cause can be seen at the bow shocks of comets. Neubauer et al. (1993) found that bow shocks at comets often are wider and more gradual than that seen at planets, which is believed to be due to mass loading. Wide quasi-perpendicular bow shocks have been observed at comet Halley by the Giotto spacecraft (Coates, 1995). Due to the low gravity of the comet, the coma extends far around the comet and affects the solar wind far upstream from the comet. Due to the similarities between Mars and comets, such as the ratio of the gyroradius compared to the scale of the system, and an extended exosphere due to weak gravitational forces, it would be possible that something similar could affect the Martian bow shock.

In this paper we study 12 wide quasi-perpendicular events in detail, and compare these with 13 thin quasi-perpendicular bow shock crossing events. We assess whether M_{MS}, a factor that affect the stand-off distance, also affect the width, and we examine whether the location on the bow shock, such as closer to the nose or the flank, affect the width. Since wide bow shocks have been seen at comets due to mass loading, the upstream ion density have been studied to see if mass loading is more present for wide bow shocks. Finally, we hypothesize that there will be more time for thermalization of ions at the wide ramps. Therefore the ion temperature has been investigated to see if the ions at wide shocks are thermalized to a larger extent than at thin shocks. Specifically, we investigate whether there is a larger difference between upstream and downstream ion temperature for the wide events than for thin events.

2 Methodology, Data and Implementation

To investigate the cause for the width, 12 wide quasi-perpendicular events and 13 thin quasi-perpendicular events have been studied. The start and end times for these events can be found in Tables. B1 and B2 in Appendix B. The amount of events was limited by time constraints of the analysis of each event, where a larger amount of events would have been impractical for in-depth analysis. There were several criteria in the event selection. The wide events had to have a width greater than 200 km, have a discernible start and end, no large upstream amplitude fluctuations such that reformation of the shock is not mistaken for width (Madanian et al., 2020), and that the angle between the IMF and the normal of the shock, θ_{bn}, had to be larger than 65°, such that they were quasi-perpendicular. Furthermore, the ramp would appear wide were the spacecraft to travel along the shock. Therefore only events where the spacecraft travelled along the normal of the bow shock were chosen (with a maximum deviation of 30°). The criteria for the thin events were the same, except their widths had to be less than 100 km. The times for the wide and thin events can be found in Table B1 and B2 respectively. Thus, the width is a criterion for the classification, and we examine the difference in other properties of the wide and thin bow shocks.

To investigate whether causes which increase stand-off distance also affect width, the Magnetosonic mach number, M_{MS} and position of each crossing was investigated and compared between the two sets of events. Furthermore, to investigate whether the abnormal width was caused by mass loading, the upstream density of protons, alpha particles and atomic and molecular oxygen ions were similarly investigated and compared. Furthermore, the increased width of the shock gives more space for the particles be accelerated or decelerated by the potential drop at the shock, which raises the question of whether the shock width affects the thermalization at the shock. To this end the ion temperature was investigated to study whether the ions at wide shocks are thermalized to a larger extent than at thin shocks. The difference between the upstream and downstream temperature for all events were calculated, and then compared between the two sets.

The data of the study is from the MAVEN spacecraft during its first dayside season, 2014-11-16 to 2015-01-04. Magnetic field data was collected by the Magnetometer (MAG) (Connerney et al., 2015) onboard. MAG measures the vectorial magnetic field at a sampling frequency of 32 samples/s, and has a resolution of 0.05 nT. Ion data was measured by the Solar Wind Ion Analyzer (SWIA) (Halekas et al., 2015), a 2π non-mass electrostatic analyzer which provides onboard calculated moments. Care has been taken to not use data during the telemetry shift of the instrument which occurs at the bow shock. The onboard calculated second moment, i.e. the temperature, is calculated under the assumption that all ions are protons. The largest error is from alpha-particles, which due to their higher mass registers as higher energy particles, thereby raising the average temperature. To investigate how large this error is we have calculated our own temperature moment from the differential energy flux measured by SWIA, and manually removed the alpha particle energy range where they have been reasonably distinguished from the protons. The resulting temperature has not varied significantly from the onboard calculated temperature, and we have therefore drawn the conclusion that the SWIA onboard calculated temperature moment can be trusted, and have used it in our study. The differential particle flux of the electron energy spectra was measured by Solar Wind Electron Analyzer (SWEA) (Mitchell et al., 2016).

The upstream ion density for specific ion populations was calculated using data from the Suprathermal and Thermal Ion Composition (STATIC) energy-mass electrostatic analyzer (McFadden et al., 2015). STATIC resolves 8 masses, 32 energies, 16 azimuthal and 4 polar angles. From the differential particle flux the ion density, velocity and temperature were calculated as the 0th, 1st and 2nd moment of the velocity distribution function respectively. All quantities are presented in the MSO coordinate system, where the positive x-axis points from Mars toward the sun, the y-axis is opposite the direction of Mars' orbital motion, and the z-axis completes the right-handed system.

As mentioned in the introduction, the angle between the IMF and the normal of the bow shock, θ_{bn}, determines the dynamics of the shock. To ensure that the bow shocks are quasi-perpendicular it has been important to accurately determine θ_{bn}. To that end, two methods have been used, the local Mixed Mode Coplanarity method (Paschmann & Schwartz, 2000), and a global bow shock model by Ramstad et al. (2017), a solar wind and EUV dependent model. According to Lepidi et al. (1997), the Mixed Mode Coplanarity method together with minimum variance analysis were the most reliable single spacecraft methods for calculating the bow shock orientation, and aligned well with the-oretical predictions. As mentioned, in order to include only quasi-perpendicular bow shocks in this study, only events where both methods gave $\theta_{bn} > 65°$ have been used.

The width of the shock was calculated by multiplying the transit time of the spacecraft passing the shock with the speed of the spacecraft along the normal. The width is therefore defined as the width in normal direction of the shock. Three methods were trialled to estimate the transit time. One method was by manual inspection, where the transit time was estimated by choosing a beginning and end of the ramp, and where care was taken to not include the foot or overshoot. The transit time was calculated under the assumption of a stationary shock. An example of ramp transit time by manual inspection can be seen in panel a) in Fig. 1, where the shaded region marks the extent of the ramp. The two other methods were curve fitting methods, where two different equations were used to fit a curve onto the data. The first function was a hyperbolic tangent function:

$$f_0(t) = s_1 + \frac{1}{2}\left(s_2 - s_1\right)\left(1 + \tanh\left(\frac{t - t_m}{\Delta t}\right)\right) \tag{1}$$

where $s_{1,2}$ are 30 second averages of the up- and downstream magnetic field magnitude, t is time, t_m is the time for the mid point of the ramp, and Δt is the transit time for the spacecraft to pass the ramp. The other function tested follows f_0 of Eq. (1) with the addition of two Gaussian functions for modeling the foot and the overshoot of the bow shock:

$$f_1(t) = f_0(t) + a_1 \exp\left(\frac{-(t - b_1)^2}{2c_1^2}\right) + a_2 \exp\left(\frac{-(t - b_2)^2}{2c_2^2}\right) \tag{2}$$

where $a_{1,2}$, $b_{1,2}$ and $c_{1,2}$ are the height, center and width respectively of the Gaussian functions. Examples of the two curve fittings can be seen in Fig. 1, where panel b) shows the curve fitting of Eq. (1), and panel c) shows the curve fitting of Eq. (2). The blue shaded regions in the figure indicate the ramp width as determined by the curve fittings. It is interesting to see that the overshoot is much smaller in amplitude and much wider than what is associated with a typical overshoot, which makes one question whether this can be called an overshoot, or if it is a different phenomenon. In the end, calculating the width by manual inspection was chosen. The curve fittings were reliable for the most part, and will be interesting to use in a future study, but at times poorly modeled the bow shock. In a set of 12 events one or two poorly modeled bow shocks would have a large effect on the results, and therefore the manual inspection method was chosen.

3 Observations

3.1 Description of example events

An example of a wide quasi-perpendicular bow shock crossing can be seen in Fig. 2. For this event θ_{bn} was 65° with the mixed-mode coplanarity method, and 74° with the model by Ramstad et al. (2017), and the width was 607 km or 19.6 r_{gi}. The transit time used for calculating this width is seen in Fig. 2 as the region marked as "Shock". The spacecraft moved from the downstream side of the shock into the upstream solar wind. At approximately time 03:07:00 in panel (a) in Fig. 2 we see a broadening of the ion energy spectrogram, with the ions starting to decelerate. Further upstream in panel (b), around 03:08:20 we see the electrons be accelerated, forming a distribution both wider in energy and with a higher bulk energy than the upstream plasma. This happens further upstream for the electrons than for the ions, since the lower electron mass makes the typical length scales shorter for the electrons. Thus, the electrons are fully thermalized further upstream than the ions. In panel (c) we see the steepening of the magnetic field, further indicating that the spacecraft is crossing the bow shock. The ion and electron spectra in panels (a) and (b), and the ion moments in panels (d-f), are measured by SWIA, which has a telemetry mode shift upon crossing into the magnetosheath. In Fig. 2 such a shift happens at 03:09:50, and for a minute around this shift the calculated

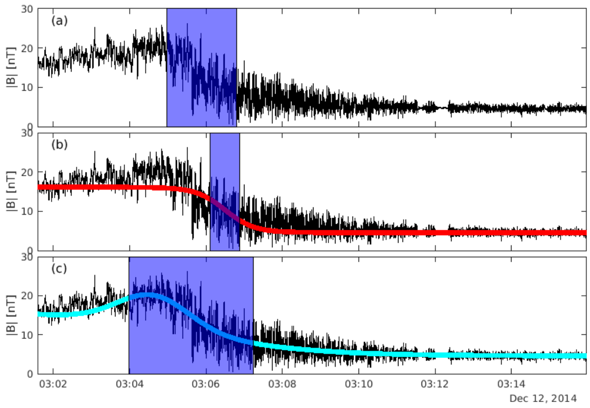

Figure 1: The three methods for determining the width of the ramp. The blue region in each panel is the ramp as determined by each method. In panel a) we see the interval that was chosen by manual inspection, in panel b) we see the curve fit of Eq. (1) and in panel c) we see the curve fit of Eq. (2).

moment will be in an ambiguous inbetween state, and should not be relied upon. We instead compare upstream and downstream ion moments to see whether the plasma has increased in density and temperature, and decreased in bulk velocity to confirm that the spacecraft has traveled into the magnetosheath. Outside ±30 s around the shift the ion moments can be trusted, it can be seen that the there is a gradual increase in density and a gradual decrease in velocity the same time we see a change in the energy spectrograms and the magnetic field. The relatively sharp increase in temperature in x-direction is likely due to the shift in telemetry mode, and for the temperature we instead look upstream and downstream for the change in temperature.

The average upstream magnetic field strength at this bow shock crossing is 4.7 nT, taken at a 30 s interval, and it is at this interval that averages for the ion density, velocity and temperature were also calculated. The regions where these values were taken can be seen in the colorbar in Fig. 2. For the temperature a downstream average was also calculated, in order to calculate the difference between the upstream and downstream temperature. The average upstream ion density was 1.85 cm^{-1}, the bulk velocity was 405 km/s, and the temperature in x-direction was 23 eV. The downstream average temperature in x-direction was 260 eV, making the ΔT of this event 237 eV. The 30 seconds of the intervals were a compromise between having a long enough averaging interval to lessen the effect of fluctuations, but not so long that too much time had passed since the bow shock crossing. The gradually increasing profiles are what characterize the wide bow shock ramp events: a broad steepening in the magnetic field and the plasma parameters. It is this behavior that is unexplained by current theory, as theory predicts that the width of a quasi-perpendicular bow shock ramp be of the size of a few electron inertial lengths (Newbury et al., 1998; le Roux et al., 2000; Hobara et al., 2010; Burne et al., 2021).

For comparison, an example of a thin quasi-perpendicular bow shock can be seen in Fig. 3. The width of this bow shock was 45 km or 6.2 r_{gi}, where the transit time used for calculating this width is seen in Fig. 3 as the region marked as "Shock". Here we see a sharp broadening of the energy spectrograms, and a sharp increase in magnetic field strength at around 04:11:40. The ion particle density and the ion bulk velocity similarly shows a quick increase and decrease respectively. For the temperature in x-direction we see an increase at the crossing and then a return to approximate solar wind temperatures. The amplitude of the magnetic field fluctuations during the shock transition are higher for the wide ramp in Fig. 2 than for the thin ramp in Fig. 3. In the case of the thin ramp (Fig. 3) there is an overshoot in both the magnetic field and density, whereas in for the wide ramp (Fig. 2) no such feature can be seen. Instead the large amplitude fluctuations in both density and magnetic field continue to be present also downstream of the shock itself. The energization of the protons and electrons are concentrated to the thin ramp, which gives less time for energization compared to the wide ramp. In the event in Fig. 3 the average upstream values of the magnetic field, ion density, velocity and temperature in x-direction was 9 nT, 5.2 cm^{-1}, 361 km/s, and 125 eV. The average downstream temperature in x-direction was 135 eV, making the ΔT of this event 10 eV.

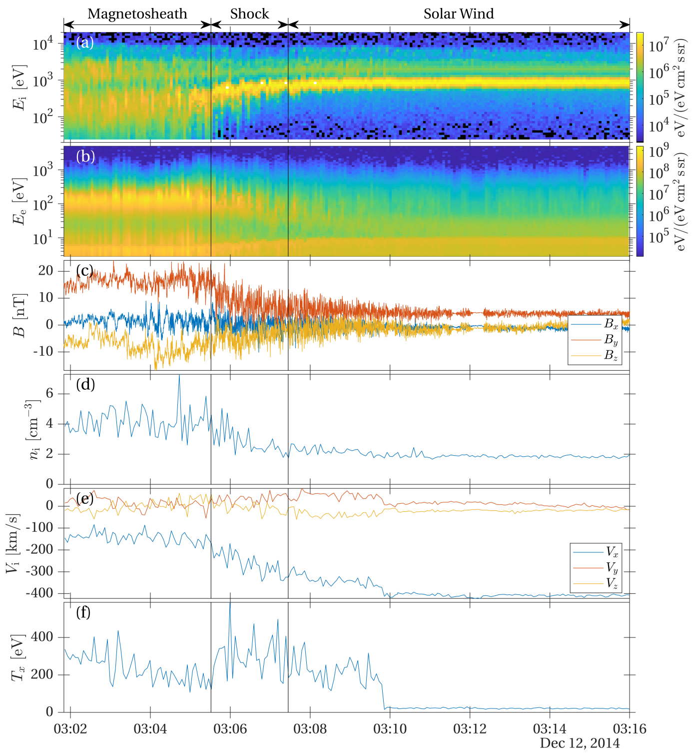

Figure 2: A wide quasi-perpendicular bow shock crossing with a width of 607 km or 19.6 r_{gi}. The spacecraft position at the time of the bow shock crossing (03:06:30) was (1.8, -0.2, 0.0)R$_M$. The panels show: a) the ion-energy spectrogram, b) the electron-energy spectrogram, (c) the magnetic field components, (d) the ion density, (e) the velocity components, and f) the temperature in x-direction.

3.2 Analysis of all events

To do some small scale statistics, 12 wide events and 13 thin events have been studied. In Fig. 4 we see where the bow shock crossings of the different events have taken place. We see an even distribution in position, with no discernible difference between wide and thin events. We do see that the majority of the bow shock crossings take place at the flank, this is likely due to orbit-bias, i.e. that MAVEN passed the bow shock at the flank during this time period. The lack of difference leads to the conclusion that the width of the ramp is not connected to location on the bow shock.

In Table 1 we see the average width and the standard deviation of the wide and thin ramps. The wide events are in the magnitude of the 100s of kilometers while the

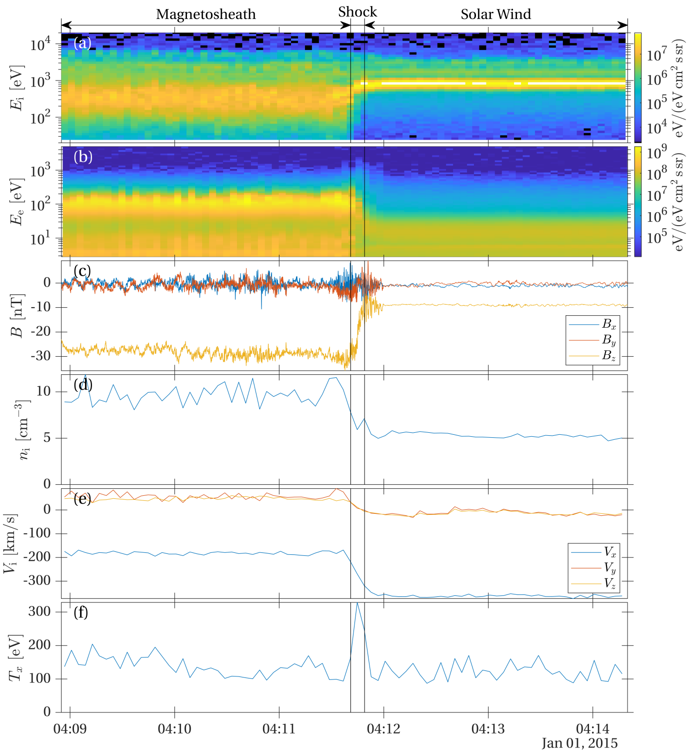

Figure 3: A thin quasi-perpendicular bow shock crossing with a width of 45 km or 6.2 r_{gi}. The spacecraft position at the time of the bow shock crossing (04:11:45) was (1.6, -1.1, 0.1)R$_M$. The panels show: a) the ion-energy spectrogram, b) the electron-energy spectrogram, (c) the magnetic field components, (d) the ion density, (e) the velocity components, and f) the temperature in x-direction.

thin events are in the 10s of kilometers. In terms of the proton gyroradius this is around 5 r_{gi} for the wide events, and 1 r_{gi} for the thin events. However the variance is very large as can be seen from the standard deviation where it is 6.7 r_{gi} for wide events and 1.6 r_{gi} for the thin events. There is however a significant difference.

It is known that the Magnetosonic Mach number, M$_{MS}$, affects stand-off distance (Edberg et al., 2010), and to see whether it also affects bow shock width we have compared M$_{MS}$ for wide and thin bow shocks. The average values of M$_{MS}$ together with one standard deviation can be found in Table 1. There were little difference to be found in M$_{MS}$ for wide and thin bow shock. Both kind of bow shocks display similar average and standard deviations in M$_{MS}$. Unlike the location of the shock, the thickness of the shock is seemingly independent of M$_{MS}$. The independence of M$_{MS}$ also aligns with the independence of location that was seen in Fig. 4, as a difference in M$_{MS}$ should correspond to a difference in bow shock stand-off distance as per previous research (Edberg et al., 2010).

In order to assess the importance of heavy ions for the nature of the shock we have computed the upstream particle densities of the ions H^+, H_2^+, O^+, and O_2^+. These can be found in Table 2. We find that the upstream particle density is higher for thin events for all ions. The average proton and atomic oxygen ion density is about twice as high, and the molecular oxygen ion density is about four times higher than for the wide events. The standard deviation is however on the scale of the average for all ions, which means there is a significant spread in density. The higher density for the thin events is not what

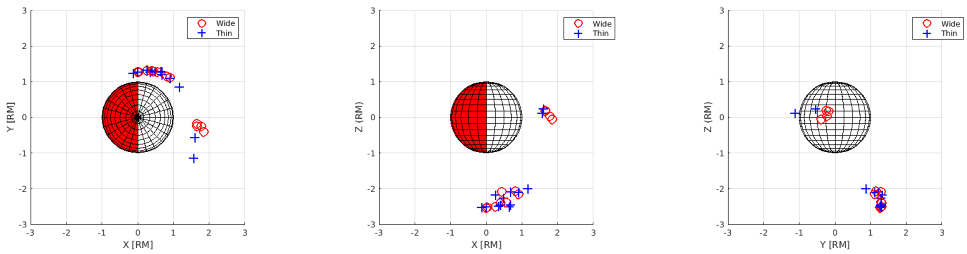

(a) YX-plane. (b) ZX-plane. (c) ZY-plane.

Figure 4: Position of bow shock crossing for the two type of events. The red circles are wide ramp events and the blue crosses are thin ramp events.

we would have expected in the case of mass loading being the cause of the wide ramps, as the higher density instead would have been expected for the wide ramps. This speaks against mass loading as being the cause of the width of the wide ramps.

Table 1: Thickness of the ramps of the wide and thin ramp events, as well as the magnetosonic Mach number. Values are given for the mean and the standard deviation (std).

	Wide		Thin	
	mean	std	mean	std
Thickness [km]	368	134	29	20
Thickness [r_{gi}]	5.4	6.7	0.7	1.6
M_{MS}	6.5	1.5	6.3	2.1

Table 2: Density of different ion species for wide and thin ramp events. Values are given for the mean and the standard deviation (std).

	Wide		Thin	
	mean	std	mean	std
H^+ [cm^{-3}]	2.5	1.9	4.4	1.9
H_2^+ [cm^{-3}]	0.2	0.1	0.3	0.2
O^+ [cm^{-3}]	0.04	0.05	0.1	0.15
O_2^+ [cm^{-3}]	0.05	0.07	0.2	0.2

Fig. 5 shows the difference between the downstream temperature and the upstream temperature in x-direction and plotted versus upstream velocity in x-direction. ΔT_x is expected to increase for increasing V_X, as there will be more energy available to be thermalized, and this can be seen for both wide and thin events. What can also be seen is that the wide events seem to more efficiently convert the kinetic energy to heat as the downstream temperatures are on average higher for the wide events. There is one outlier with a $\Delta T_x = 240$ eV, but even with that removed the average is higher. This is especially interesting given that the thin events had higher average upstream ion particle density, as that would imply there is more kinetic energy available. The higher energy transport for the wide events could be interesting for ionization of particles and particle escape, as it could implicate that more particles could be ionized and/or reach escape velocity.

4 Discussion

A caveat for this study is that it has been conducted under the assumption of a non-moving shock. Due to the limitations of single-spacecraft measurements it is difficult to estimate the movement of the shock. Methods such as estimating the velocity from the foot (Burne et al., 2021) has not been used here due to the difficulty in distinguishing the foot in the wide ramp events. This makes this line of questioning an excellent one to continue with multi-point measurements, this study aims to open the discussion of the width of the shock.

In spite of this being a single spacecraft study, one can have confidence that the wide shocks are indeed wide. A bow shock that rapidly moves back and forth would result in multiple bow shock crossings, which indeed can be observed in cases not included in this study. For a thin shock to be misinterpreted as a wide shock as those studied here, it would have to move at a speed just slightly faster than, and synchronised with, the spacecraft speed over the course of several minutes, and that is not likely. For example if a thin bow shock is 30 km wide, and the duration of the crossing of a wide shock is 3 minutes, then the relative spacecraft–bow shock velocity would have to be 0.17 km/s, which is much smaller than the typical spacecraft speed of 1.5-3 km/s at the bow shock. Could the opposite hypothesis be true: that all shocks are wide, some masked as thin by passing the spacecraft very quickly? This would require the bow shock to move in the range of 100 km/s which is possible. However, such a motion would not explain the differences in other properties between the shock types, such as fluctuation amplitudes and the presence or absence of an overshoot.

The cause for the bow shock thickness to differ between the different cases remains an open question. It is well known that the quasi-parallel and quasi-perpendicular shocks differ with the quasi-parallel having an extensive foreshock region, which potentially could be interpreted as a wider shock. In this study only quasi-perpendicular shocks are included, and therefore the difference between the parallel and perpendicular shocks cannot explain the observations. At comets, mass loading is important in determining the standoff distance of the bow shock (e.g., Koenders et al., 2013). The bow shocks encountered in the fast flybys of comets in the 1980s and 90s also had large widths. While this could lead to the speculation that the presence of heavy ions increases the bow shock width, that hypothesis cannot be confirmed by our data from Mars. As Table 2 shows, the density of heavy planetary ions is lower for the wide than for the thin shocks.

There is a potential across the shock, which slows the solar wind ions down while accelerating the electrons. The electron energy can be used to estimate this potential drop (Xu et al., 2021). It is seen in Figs. 2 and 3 that the energy of electrons and ions vary in the same way as the other quantities. The energy changes over a short distance for the thin ramps and over an outstretched region in the case of the wide ramps. This implies that also the potential drop changes over an extended region for the wide ramps and that the potential drop is concentrated in a thin layer for the thin ramps. The amplitude of the waves present is higher for the wide than thin ramps, and we suggest that in the wide ramps the waves may be able to balance the wider potential drop.

5 Summary

In this study wide quasi-perpendicular bow shocks have been compared to thin quasi-perpendicular bow shocks. The characteristics of the wide bow shocks show no difference in dependence of the bowshock's location with respect to the planet (sub-solar or flank) nor with respect to the magnetosonic Mach number. The wide bow shock events show lower upstream density than their thin counterparts, for protons, alpha particles, and atomic and molecular oxygen. With this in mind it is particularly interesting that they show a higher difference in upstream and downstream temperature, implying a higher

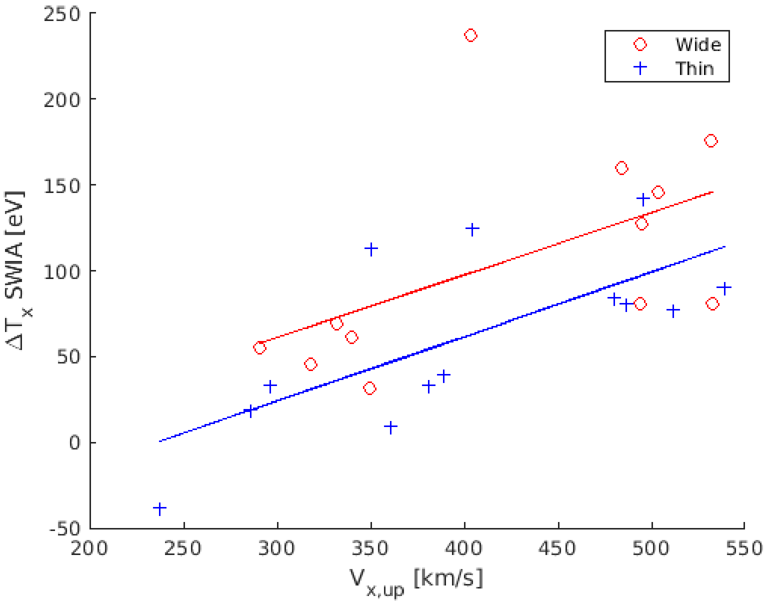

Figure 5: Difference in upstream and downstream temperature in x-direction for all events, $\Delta T_x = T_{down}$ - T_{up} over $V_{x,up}$.

rate of energy transfer at the wide bow shock. Future studies could look into larger amount of events, study the potential drop at the ramp, and perform wave analysis to see how waves affect the width of the shock. It will be of particular interest when multi-point measurements at Mars become available, as it will resolve some of the ambiguity of the shock movement and velocity. This study shows that current theory cannot fully describe the processes at the bow shock at Mars, and that these conditions affect not only bow shock width, but also increases the thermalization of ions at the Martian shock.

Appendix A Comparison between the quasi-parallel and quasi-perpendicular bow shock

To illustrate the difference between a wide quasi-perpendicular and a wide quasi-parallel bow shock we show a crossing of a wide quasi-parallel ramp in Fig. A1, which has $\theta_{bn} = 24°$ and $29°$ for the local and model method respectively. Due to the lack of discernible start and end of the ramp, it is hard to estimate the width, but an approximate value for this shock would be around 450 km. An important difference between wide quasi-parallel bow shock ramps and quasi-perpendicular ones is the amount of wave activity. At quasi-parallel bow shocks particles are reflected and escape upstream along the magnetic field lines, creating an extensive foreshock region. Due to the available free energy from the reflected particle beam there will be a multitude of instabilities and waves, and the solar wind will begin to be decelerated upstream of the bow shock. This makes the ramp appear very wide, often with no discernible start and end. At the quasi-perpendicular bow shock the reflected particles only reflect at most a gyroradius, and as such the solar wind in front of the shock less disturbed. At quasi-perpendicular bow shocks we can often discern a foot and an overshoot, coming from the reflected particles and sheet current respectively. These are not present at quasi-parallel shocks. In Fig. 2 we can see a wide quasi-perpendicular shock, with a wide ramp, but a discernible start and end, and a slight overshoot, though small. At the wide quasi-parallel shock in Fig. A1 there is large amplitude wave activity upstream and downstream, it is difficult to discern a beginning and end of the ramp, and no foot or overshoot can be identified.

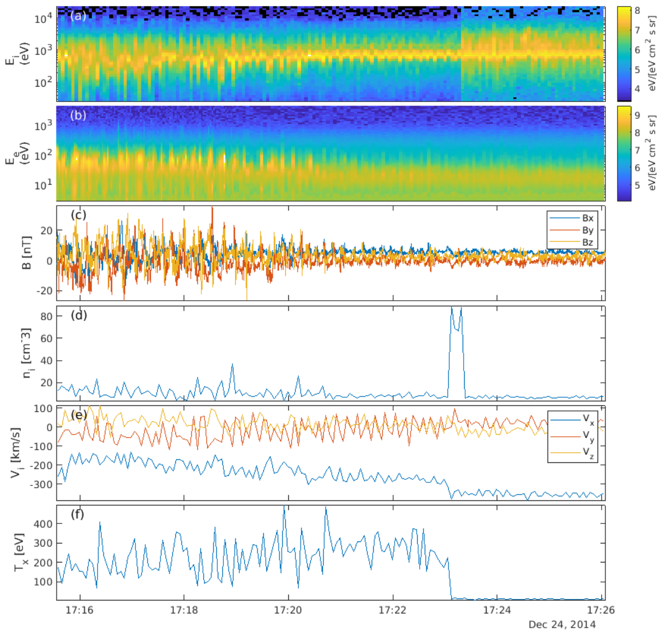

Figure A1: An approximately 450 km wide quasi-parallel bow shock crossing. The panels show: a) the ion-energy spectrogram, b) the electron-energy spectrogram, (c) the magnetic field components, (d) the ion density, (e) the velocity components, and f) the temperature in x-direction.

Appendix B Event start and end times

Table B1: Start and end times for wide events

Start event	End event
2014-12-03 09:58:56	2014-12-03 10:20:06
2014-12-04 22:45:55	2014-12-04 23:04:04
2014-12-07 05:29:28	2014-12-07 06:11:47
2014-12-08 21:00:49	2014-12-08 21:12:24
2014-12-10 09:42:36	2014-12-10 09:53:27
2014-12-12 03:01:35	2014-12-12 03:15:58
2014-12-15 11:04:47	2014-12-15 11:19:30
2014-12-16 17:06:30	2014-12-16 17:15:04
2014-12-18 07:46:08	2014-12-18 08:01:48
2014-12-29 00:42:09	2014-12-29 00:56:47
2015-01-02 14:29:10	2015-01-02 14:48:57
2015-01-04 07:40:40	2015-01-04 08:05:06

Table B2: Start and end times for thin events

Start event	End event
2014-11-16 13:09:23	2014-11-16 13:14:41
2014-12-03 01:02:37	2014-12-03 01:06:57
2014-12-05 03:29:22	2014-12-05 03:38:14
2014-12-05 16:46:07	2014-12-05 17:04:38
2014-12-12 14:09:29	2014-12-12 14:26:38
2014-12-13 03:48:06	2014-12-13 04:04:02
2014-12-17 15:52:56	2014-12-17 15:57:55
2014-12-22 22:00:06	2014-12-22 22:11:06
2014-12-23 07:16:52	2014-12-23 07:24:27
2015-01-01 04:08:52	2015-01-01 04:14:25
2015-01-01 15:43:13	2015-01-01 16:01:55
2015-01-04 03:13:54	2015-01-04 03:26:23
2015-01-13 16:07:22	2015-01-13 16:17:46

Acknowledgments

All MAVEN data are publicly available through the Planetary Data System (https://pds-ppi.igpp.ucla.edu/).

This work was funded by the Swedish National Space Board (SNSA, projects 108/18 and 194/19).

The authors would like to thank students J. Eriksson, E. Johansson, E. Rantala, P Sehlstedt, and F. Wikner at Umeå University for their development of the curve fitting method of Eq. (2).

References

Bale, S. D., Balikhin, M. A., Horbury, T. S., Krasnoselskikh, V. V., Kucharek, H., Möbius, E., ... Thomsen, M. F. (2005, Jun 01). Quasi-perpendicular shock structure and processes. *Space Science Reviews*, *118*(1), 161–203. Retrieved from `https://doi.org/10.1007/s11214-005-3827-0` doi: 10.1007/s11214-005-3827-0

Balikhin, M., Krasnosselskikh, V., & Gedalin, M. (1995). The scales in quasiperpendicular shocks. *Advances in Space Research*, *15*(8), 247-260. Retrieved from `https://www.sciencedirect.com/science/article/pii/027311779400105A` (Proceedings of the D2.1 Symposium of COSPAR Scientific Commission D) doi: https://doi.org/10.1016/0273-1177(94)00105-A

Balogh, A., & Treumann, R. A. (2013). *Physics of collisionless shocks* (Vol. 12). Springer, New York, NY. doi: 10.1007/978-1-4614-6099-2

Behannon, K. W. (1968). Mapping of the earth's bow shock and magnetic tail by explorer 33. *Journal of Geophysical Research (1896-1977)*, *73*(3), 907-930. Retrieved from `https://agupubs.onlinelibrary.wiley.com/doi/abs/10.1029/JA073i003p00907` doi: https://doi.org/10.1029/JA073i003p00907

Burne, S., Bertucci, C., Mazelle, C., Morales, L. F., Meziane, K., Halekas, J., ... Penou, E. (2021). The structure of the Martian quasi-perpendicular supercritical shock as seen by MAVEN. *Journal of Geophysical Research (Space Physics)*,

126(9), e2020JA028938. doi: 10.1029/2020JA028938
Coates, A. J. (1995, March). Heavy ion effects on cometary shocks. *Advances in Space Research*, *15*(8-9), 403–413. doi: 10.1016/0273-1177(94)00125-K
Connerney, J. E. P., Espley, J., Lawton, P., Murphy, S., Odom, J., Oliversen, R., & Sheppard, D. (2015). The maven magnetic field investigation. *Space Sci Rev*, *195*, 257–291. doi: https://doi.org/10.1007/s11214-015-0169-4
Edberg, N. J. T., Lester, M., Cowley, S. W. H., Brain, D. A., Fränz, M., & Barabash, S. (2010). Magnetosonic mach number effect of the position of the bow shock at mars in comparison to venus. *Journal of Geophysical Research: Space Physics*, *115*(A7). Retrieved from `https://agupubs.onlinelibrary.wiley.com/doi/abs/10.1029/2009JA014998` doi: https://doi.org/10.1029/2009JA014998
Farris, M. H., & Russell, C. T. (1994). Determining the standoff distance of the bow shock: Mach number dependence and use of models. *Journal of Geophysical Research: Space Physics*, *99*(A9), 17681-17689. Retrieved from `https://agupubs.onlinelibrary.wiley.com/doi/abs/10.1029/94JA01020` doi: https://doi.org/10.1029/94JA01020
Halekas, J. S., Taylor, E. R., Dalton, G., Johnson, G., Curtis, D. W., McFadden, J. P., ... Jakosky, B. M. (2015). The solar wind ion analyzer for maven. *Space Sci Rev*, *195*, 125–151. doi: https://doi.org/10.1007/s11214-013-0029-z
Hobara, Y., Balikhin, M., Krasnoselskikh, V., Gedalin, M., & Yamagishi, H. (2010). Statistical study of the quasi-perpendicular shock ramp widths. *Journal of Geophysical Research: Space Physics*, *115*(A11). Retrieved from `https://agupubs.onlinelibrary.wiley.com/doi/abs/10.1029/2010JA015659` doi: https://doi.org/10.1029/2010JA015659
Koenders, C., Glassmeier, K.-H., Richter, I., Motschmann, U., & Rubin, M. (2013, October). Revisiting cometary bow shock positions. *Planet. Space Sci.*, *87*, 85–95. doi: 10.1016/j.pss.2013.08.009
Lepidi, S., Villante, U., & Lazarus, A. J. (1997). Single spacecraft identification of the bow shock orientation and speed: A comparison between different methods. *Il nuovo cimento*, *20*(6), 911-922. Retrieved from `http://eprints.bice.rm.cnr.it/id/eprint/12401`
le Roux, J. A., Fichtner, H., Zank, G. P., & Ptuskin, V. S. (2000). Self-consistent acceleration of multiply reflected pickup ions at a quasi-perpendicular solar wind termination shock: a fluid approach. *Journal of Geophysical Research: Space Physics*, *105*(A6), 12557-12577. Retrieved from `https://agupubs.onlinelibrary.wiley.com/doi/abs/10.1029/1999JA000273` doi: https://doi.org/10.1029/1999JA000273
Luhmann, J., Ledvina, S., & Russell, C. (2004). Induced magnetospheres. *Advances in Space Research*, *33*(11), 1905-1912. Retrieved from `https://www.sciencedirect.com/science/article/pii/S0273117704000158` (Comparative Magnetospheres) doi: https://doi.org/10.1016/j.asr.2003.03.031
Madanian, H., Schwartz, S. J., Halekas, J. S., & Wilson III, L. B. (2020). Nonstationary quasiperpendicular shock and ion reflection at Mars. *Geophys. Res. Lett.*, *47*(11), e2020GL088309. doi: 10.1029/2020GL088309
McFadden, J. P., Kortmann, O., Curtis, D., Dalton, G., Johnson, G., Abiad, R., ... M., J. (2015). Maven suprathermal and thermal ion compostion (static) instrument. *Space Sci Review*, *195*, 199–256. doi: https://doi.org/10.1007/s11214-015-0175-6
Mitchell, D. L., Mazelle, C., Sauvaud, J.-A., Thocaven, J.-J., Rouzaud, J., Fedorov, A., ... Jakosky, B. M. (2016). The maven solar wind electron analyzer. *Space Sci Review*, *200*, 495–528. doi: https://doi.org/10.1007/s11214-015-0232-1
Neubauer, F. M., Marschall, H., Pohl, M., Glassmeier, K.-H., Musmann, G., Mariani, F., ... Ungstrup, E. (1993, February). First results from the Giotto magnetometer experiment during the P/Grigg-Skjellerup encounter. *Astron-*

omy & Astrophysics, *268*, L5–L8.

Newbury, J. A., Russell, C. T., & Gedalin, M. (1998). The ramp widths of high-mach-number, quasi-perpendicular collisionless shocks. *Journal of Geophysical Research: Space Physics*, *103*(A12), 29581-29593. Retrieved from `https://agupubs.onlinelibrary.wiley.com/doi/abs/10.1029/1998JA900024` doi: https://doi.org/10.1029/1998JA900024

Parks, G. (2015). Magnetosphere. In G. R. North, J. Pyle, & F. Zhang (Eds.), *Encyclopedia of atmospheric sciences (second edition)* (Second Edition ed., p. 309-315). Oxford: Academic Press. Retrieved from `https://www.sciencedirect.com/science/article/pii/B9780123822253002115` doi: https://doi.org/10.1016/B978-0-12-382225-3.00211-5

Paschmann, G., & Schwartz, S. J. (2000, February). ISSI Book on Analysis Methods for Multi-Spacecraft Data. In R. A. Harris (Ed.), *Cluster-ii workshop multiscale / multipoint plasma measurements* (Vol. 449, p. 99).

Ramstad, R., Barabash, S., Futaana, Y., & Holmström, M. (2017). Solar wind- and euv-dependent models for the shapes of the martian plasma boundaries based on mars express measurements. *Journal of Geophysical Research: Space Physics*, *122*(7), 7279-7290. Retrieved from `https://agupubs.onlinelibrary.wiley.com/doi/abs/10.1002/2017JA024098` doi: https://doi.org/10.1002/2017JA024098

Valek, P. W., Thomsen, M. F., Allegrini, F., Bagenal, F., Bolton, S., Connerney, J., … Wilson, R. J. (2017). Hot flow anomaly observed at jupiter's bow shock. *Geophysical Research Letters*, *44*(16), 8107-8112. Retrieved from `https://agupubs.onlinelibrary.wiley.com/doi/abs/10.1002/2017GL073175` doi: https://doi.org/10.1002/2017GL073175

Xu, S., Schwartz, S. J., Mitchell, D. L., Horaites, K., Andersson, L., Halekas, J., … Gruesbeck, J. R. (2021). Cross-shock electrostatic potentials at Mars inferred from MAVEN measurements. *Journal of Geophysical Research: Space Physics*, *126*(3), e2020JA029064. doi: 10.1029/2020JA029064